OPEN ACCESS

University of Dundee

University of Dundee

Viscoelastic properties' characterization of corneal stromal models using non-contact surface acoustic wave optical coherence elastography (SAW-OCE)

Zhang, Yilong; Zhou, Kanheng; Feng, Zhengshuyi; Feng, Kairui; Ji, Yubo; Li, Chunhui

Published in:
Journal of Biophotonics

DOI:
10.1002/jbio.202100253

Publication date:
2022

Document Version
Peer reviewed version

Link to publication in Discovery Research Portal

Citation for published version (APA):
Zhang, Y., Zhou, K., Feng, Z., Feng, K., Ji, Y., Li, C., & Huang, Z. (2022). Viscoelastic properties' characterization of corneal stromal models using non-contact surface acoustic wave optical coherence elastography (SAW-OCE). *Journal of Biophotonics*, *15*(1), 1-13. Article e202100253. Advance online publication. https://doi.org/10.1002/jbio.202100253

General rights
Copyright and moral rights for the publications made accessible in Discovery Research Portal are retained by the authors and/or other copyright owners and it is a condition of accessing publications that users recognise and abide by the legal requirements associated with these rights.

- Users may download and print one copy of any publication from Discovery Research Portal for the purpose of private study or research.
- You may not further distribute the material or use it for any profit-making activity or commercial gain.
- You may freely distribute the URL identifying the publication in the public portal.

Take down policy
If you believe that this document breaches copyright please contact us providing details, and we will remove access to the work immediately and investigate your claim.

Download date: 12. Oct. 2023

Accepted Article

Title: Viscoelastic properties characterisation of corneal stromal models using non-contact surface acoustic wave optical coherence elastography (SAW-OCE)

Yilong Zhang, Kanheng Zhou, Zhengshuyi Feng, Kairui Feng, Yubo Ji, Chunhui Li*, and Zhihong Huang

School of Science and Engineering, University of Dundee, Dundee DD1 4HN, Scotland, UK

*Correspondence
Chunhui Li, School of Science and Engineering, University of Dundee, Dundee DD1 4HN, Scotland, UK
Email: C.Li@dundee.ac.uk

This article has been accepted for publication and undergone full peer review but has not been through the copyediting, typesetting, pagination and proofreading process which may lead to differences between this version and the Version of Record. Please cite this article as doi: 10.1002/jbio.202100253

This article is protected by copyright. All rights reserved.

Accepted Article

Abstract

Viscoelastic characterisation of the tissue-engineered corneal stromal model is important for our understanding of the cell behaviours in the pathophysiologic altered corneal extracellular matrix (ECM). The effects of the interactions between stromal cells and different ECM characteristics on the viscoelastic properties during an 11-day culture period were explored. Collagen-based hydrogels seeded with keratocytes were used to replicate human corneal stroma. Keratocytes were seeded at 8×10^3 cells per hydrogel, and collagen concentrations of 3, 5 and 7 mg/ml. An air-pulse-based surface-acoustic-wave optical coherence elastography (SAW-OCE) was employed to monitor the changes in the hydrogels' dimensions and viscoelasticity over the culture period. The results showed the elastic modulus increased by 111%, 56% and 6%, and viscosity increased by 357%, 210% and 25% in the 3, 5 and 7 mg/ml hydrogels respectively. To explain the SAW-OCE results, scanning electron microscope (SEM) was also performed. The results confirmed the increase in elastic modulus and viscosity of the hydrogels respectively arose from increased fibre density and force-dependent unbinding of bonds between collagen fibres. This study reveals the influence of cell-matrix interactions on the viscoelastic properties of corneal stromal models and can provide quantitative guidance for mechanobiological investigations which require collagen ECM with tuneable viscoelastic properties.

Keywords: air-pulse system, corneal stromal model, cell-matrix interactions, optical coherence elastography (OCE), surface acoustic wave (SAW), viscoelastic properties

This article is protected by copyright. All rights reserved.

Accepted Article

1 INTRODUCTION

The cornea plays a major role in human vision by contributing about two-thirds optical power of the eye. It also acts as a structural barrier and protects the eye from infections [1]. The corneal biomechanical properties are closely related to its physio-pathological conditions, which are important to access the development of corneal diseases, the surgical and therapeutic outcomes [2]. For instance, in keratoconus, the cornea exhibits reduced elastic modulus, decreased thickness and pathological weakening, resulting in corneal bulging, and severe visual degradation [3, 4]. Meanwhile, varied stress distribution of the cornea leads to altered viscoelastic behaviours, which may give rise to corneal ectasia occurring in Keratoconus [5]. However, characterising the biomechanical properties of the cornea is a challenge due to the nonlinear viscoelastic behaviours of the cornea and non-invasive measurements required. The Ocular Response Analyser (ORA) [6, 7] is a clinical approach that applies a large volume air impulse to displace the corneal surface, and then quantify corneal hysteresis, a viscoelastic parameter of the cornea. However, only the viscoelastic property of the entire cornea can be measured in this approach and there is a disagreement regarding its ability to detect the biomechanical changes in keratoconus eyes before and after the cross-linking treatments compared to pathological or therapeutic outcomes [5, 8, 9]. In addition, little is known about the altered viscoelasticity of corneal extracellular matrix (ECM) interaction with cells, and the morphological changes of collagen fibres in the ECMs with various viscoelastic characteristics.

The biomechanical characteristics of the cornea are mainly derived from the stroma, a connective tissue contributing about 85% of the total thickness of the cornea [1]. *In vitro* examinations are able to investigate a specific biomechanical property and control certain experimental situations in corneal equivalents, especially in studying the relationship between cells and stromal ECM in a reconstructed corneal stroma model [10]. As a typical scaffold material, hydrogels have been widely used in tissue engineering applications. These materials can provide a biomimetic three-dimensional (3D) microenvironment for cell growth, relying on

This article is protected by copyright. All rights reserved.

Accepted Article

their tissue-mimicking characteristics, biocompatibility, and tuneable biomechanical properties [11]. Collagen is the primary natural protein of the corneal stroma, playing an important role in maintaining corneal structural integrity and transparency [12]. Of all the types of collagens, type I collagen is the most abundant ECM composition in the stroma [13]. Keratocytes, also known as human corneal fibroblasts, are the main cell type of human corneal stroma and are sparsely distributed in the stroma. The primary function of keratocytes is to regulate the collagen scaffold and ECM of the stroma [14]. Thus, collagen-based hydrogels incorporated with keratocytes are ideal for replicating the human corneal stroma as their compositions and viscoelastic properties are similar to the real stroma [15]. On the other hand, characterising the viscoelasticity of collagen-based hydrogels will allow quantitative guiding mechanobiological investigations of wound healing [16], cancer metastasis [17], etc., which requires collagen ECM with tuneable mechanical properties.

To date, the elastic modulus (Young's modulus) of collagen-based constructs in cell biology have been well illustrated. Explicitly, cells change the mechanical characteristics of collagen hydrogels through releasing ECM products and digestion enzymes [18]. Moreover, attachment and integration of cells within the hydrogels [19], lead to contraction of the hydrogels [20]. In turn, the altered stiffness of the ECM can influence viability, migration [21], differentiation [22] and proliferation [23] of cells. However, collagen matrix is not just elastic, but also viscous, which exhibits a time-dependent mechanical response. The impacts of the collagen ECM viscosity on cell behaviours remain unclear, although Chaudhuri *et al.* [24] reported that cell proliferation, spreading and differentiation were regulated by the different viscosity of the collagen matrix. However, cell responses to viscous ECMs are largely uncharacterised as the cell-matrix altered viscoelasticity is lacking for quantitative studies. The viscoelastic properties of the collagen matrix probably can be explained with respect to collagen fibres. In weakly cross-linked collagen hydrogels, the fibre density determines matrix stiffness [25, 26]. A reasonable explanation of the change in viscosity was proposed by Nam *et al.*, where he stated that

This article is protected by copyright. All rights reserved.

Accepted Article

artificially strain-enhanced viscosity resulted from force-dependent unbinding of bonds between fibres in such hydrogels [27]. However, the viscoelastic property changes in hydrogels resulting from the morphological changes of fibres in collagen ECM due to the cell-matrix interactions have never been studied. Therefore, it is important to interpret the quantitative viscoelasticity of the collagen-based constructs resulting from cell-matrix behaviours.

The basic approaches to examine the viscoelastic properties of tissue-engineered materials are the stress relaxation test [28, 29] and the creep test [28, 30]. Nowadays, rheometers have become popular to quantify the viscoelasticity of the engineered materials, and shear stresses and strains of tested samples are being measured by this method [31-33]. Nevertheless, all these techniques are destructive to the engineered tissues. Hence, a non-destructive and non-contact technology is needed to quantify and continuously monitor the biomechanical properties of the engineered constructs.

Optical coherence tomography (OCT) has been a popular imaging modality that enables non-invasive imaging of biological soft tissues with high spatial and temporal resolutions [34]. By applying external stimulations, OCT can turn into a useful technique for characterising the biomechanical properties of soft tissues, termed optical coherence elastography (OCE) [35, 36]. Among various types of OCE techniques, air-pulse-based surface acoustic wave OCE (SAW-OCE) is a completely non-contact stimulation technique developed by Wang *et al.*[37]. In this method, a SAW impulse was first generated on the sample surface through a transient air stream, and a phase-sensitive optical coherence tomography (PhS-OCT) system was then used to track the generated SAW pulse. The mechanical property of the sample was obtained by fitting the SAW phase velocity dispersion curve into its corresponding dispersion model. As reported previously, air-pulse-based SAW-OCE has been used to characterise the elasticity [37] and the viscoelasticity [38] of soft tissues. With regards to the cornea, Air-pulse OCE had favourable applications in characterising the corneal elasticity [39, 40]. It has also been reported to quantitatively assess corneal viscoelasticity [41, 42]. To our knowledge, this is the first study

This article is protected by copyright. All rights reserved.

Accepted Article

monitoring the changes in viscoelastic properties of tissue-engineered tissue by using air-pulse-based SAW-OCE.

In order to understand the influence of the interactions between stromal cell and stromal ECM on the viscoelastic property of the corneal stroma models, changes in the dimensions and the viscoelastic properties of the hydrogels with different initial collagen concentrations were monitored by a focused air-pulse induced SAW-OCE method over a consecutive 11-day culture period. The morphological alterations in collagen fibres in the hydrogels, including the fibre density and fibre diameter, were also examined using scanning electron microscope (SEM) to explore the relationship between fibre properties and viscoelasticity of the hydrogels with different initial collagen concentrations.

2 Materials and Methods

2.1 Human corneal stroma mimicking hydrogel preparation

Keratocytes (P10872, Innoprot, Bizkaia, Spain) at the 3rd passage were cultured in a T25 cell culture flask with 5 ml culture media composed of low glucose Dulbecco's Modified Eagle's Medium (DMEM, 1.0 g/L glucose, Lonza, Basel, Switzerland) supplemented by 10% Foetal Bovine Serum (FBS, Thermo Fisher Scientific Inc., Massachusetts, USA), and 1% antibiotic and antimitotic solution (PEN-STREP 5000 U Penicillin/m, 5000U Streptomycin/ml, Lonza, Basel, Switzerland) in an incubator with 5% carbon dioxide (CO_2) at 37 °C. The culture media was refreshed every 2 days. Hydrogel samples with a total value of 80 µL were prepared with rat-tail collagen type I (9.1 mg/ml, CORNING, New York, USA) following a previously reported protocol [43]. When keratocytes reached a confluency of 80% in the culture flask, these cells were trypsinised, and then counted by a hemacytometer. Next, keratocytes were suspended within the hydrogel solution and transferred to a cellulose ring (inner diameter of 5 mm and outer diameter of 8 mm) for gelation, resulting in the final hydrogel sample with a dome shape. Hydrogels with collagen concentrations of 3 mg/ml, 5 mg/ml and 7 mg/ml and cell

This article is protected by copyright. All rights reserved.

concentration of 1×10^5 cells/ml were manufactured for both SAW-OCE and SEM experiments at the same time. Hydrogels without cells were produced as a control. Each type of hydrogel had three and two repeats, respectively. The hydrogels were individually cultured in a 35-mm petri dish with 3 ml culture media in the incubator.

2.2 Cell confluency and morphology in hydrogels

A higher cell number in hydrogel leads to a faster increase in elastic modulus and a higher modulus value of hydrogel [44], through influencing the cell density and the amount of contraction of hydrogel [45]. To qualitatively monitor the cell proliferation process, the confluency, and the morphology of keratocytes in the cell-seeded hydrogels with initial collagen concentrations of 3 mg/ml, 5 mg/ml and 7 mg/ml were observed with a light microscope (Olympus CKX41, Olympus Tokyo, Japan) at a magnification of 100× every 24 h.

2.3 Air-pulse-based SAW-OCE system

A SAW-OCE system consists of a customised air-pulse system and a phase-sensitive optical coherence tomography (PhS-OCT) system. **Figure 1** illustrates a schematic diagram of the air-pulse system with the explanation of inducing the SAW in the hydrogel samples (Figure 1A) and synchronous acquisition of the SAW by the PhS-OCT (Figure 1B). The setup of focused air-pulse system was clearly described in a previous publication [37]. In this study, the customised air-pulse system relied on a pneumatic solenoid value (V114-6M-M5, SMC Corporation, Tokyo, Japan) and a customised control circuit that was used to manage the duration of an air stream. The output signal from the control part in the air-pulse system implemented the synchronisation with the PhS-OCT system.

The air pressure was adjusted by a pressure control value and read through a pressure meter on an air compressor (Tayside compressor services, Dundee, UK). A needle (0.15 mm, KDS3012P, Weller, Besigheim, Germany) was used as an air outlet. The position of the needle was precisely adjusted with a 3D translation stage for localised air-pulse excitation. The air-pulse system was

This article is protected by copyright. All rights reserved.

Accepted Article

Accepted Article

driven by an externally triggered function generator (33220A, Keysight Technologies Inc., California, USA). The driving signal was a square wave with a frequency of 40 Hz, an amplitude of 5.0 volts peak-to-peak (Vpp), with an offset of +2.5 volts direct current (V_{dc}), and a duty cycle of 60%. The needle tip was placed at the left of the hydrogels and the excitation angle of incidence relative to the surface normal of the hydrogels was set to 45°. The air pressure was set to 1 bar, inducing the SAW pulse with the maximum amplitude of 250 nm on the surface of the hydrogels. To avoid phase wrapping, the distance between needle tip and surface of the hydrogels was set to 0.55 mm. The impulse SAW was acquired by the PhS-OCT system and the data was recorded by LabVIEW (V2016, National Instruments, Texas, USA) programme.

The PhS-OCT as a spectrum-domain OCT (SD-OCT) was utilised for the acquisition of the SAW induced by the air-pulse system. The PhS-OCT system was composed of a broadband laser source (a central wavelength of 1310 nm, bandwidth of ~83 nm, and output power of ~10 Mw, LS2000B), a 90/10 beam splitter, a stational reference arm, a sample arm combined with a 2D galvo-scanner and a high-speed spectrometer (linear InGaAs camera, Sensors Unlimited Inc., New Jersey, USA). The optical power emitted from the sample arm was measured to be 8.51 mW. The phase stability of this system in sample is around 60 milliradian (mrad), which can detect the minimal axial displacement of ~6 nm. The maximum sampling frequency of our system can reach 91,912 Hz. The lateral and axial resolution of the system in air was ~16 μm and ~5.8 μm, respectively.

The central cross-sectional plane of each hydrogel was selected for imaging. An M-B scanning protocol was employed to acquire the propagation of the impulse SAW. In this mode, 512 A-scans were taken at the same location with a sampling frequency of 20,730 Hz, forming a M-scan first. Then, 512 consecutive M-scans with a lateral spacing of 17 μm were acquired horizontally with a frame rate of 30 Hz, forming one complete M-B scan within 18.9 s. The size of effective imaging plane was ~2.4 mm × ~9 mm (depth × lateral distance). The PhS-OCT system was synchronised with the air-pulse system at each M-scan by an external trigger signal.

This article is protected by copyright. All rights reserved.

Each set of 4 M-B scans was averaged to generate a composed M-B scan for signal-to-noise ratio (SNR) enhancement. Thus, the total acquisition time for each hydrogel sample was approximately 75.6 s.

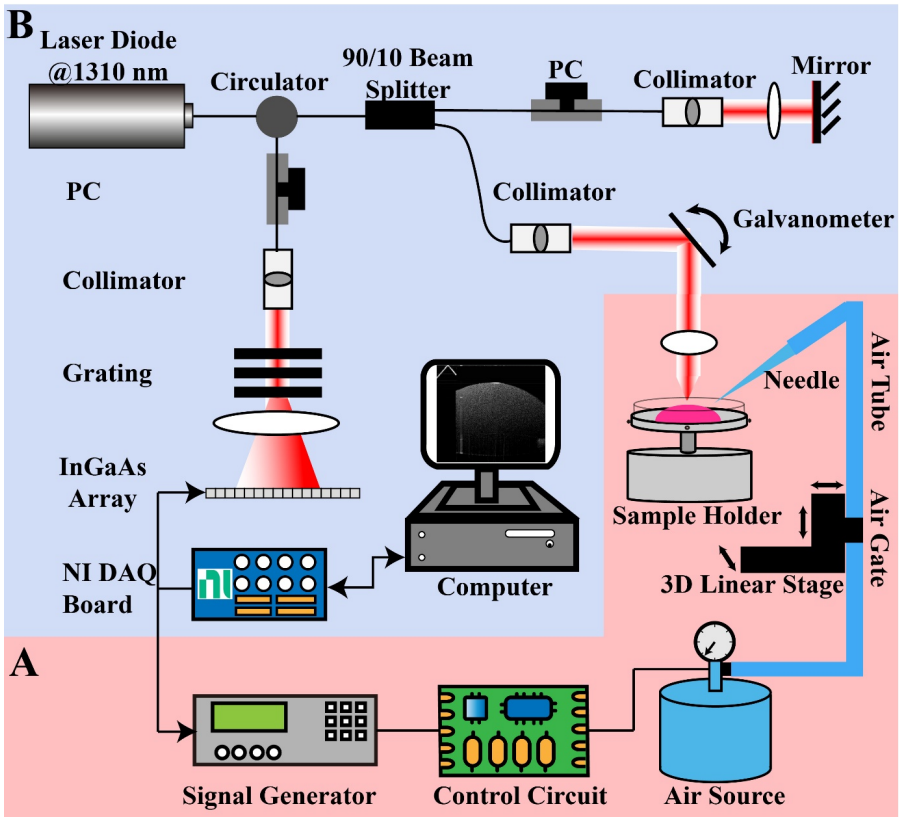

Figure 1. A schematic of an air-pulse induced SAW-OCE system consisting of an air-pulse generation part (A. pink) and a PhS-OCT system (B. blue). PC: Polarization Controller. NI: national instrument. DAQ: Data acquisition.

2.4 Central thickness measurements

The cross-sectional thickness is another indicator that can directly reflect the contraction of the hydrogels, which affects their mechanical properties by removing water content [46]. The thickness of the centre cross-sectional plane of each hydrogel was non-destructively examined by the PhS-OCT system every other day. The method was described in our previous study [47]. In brief, the central thickness of the hydrogel was calculated by the pixel numbers from peak to bottom of the hydrogels in the centre cross-sectional plane, then multiplied by the length of each pixel. Due to water content in the hydrogels over 99%, the refractive index of the hydrogels

This article is protected by copyright. All rights reserved.

Accepted Article

was assumed the same as water, at 1.333 [48]. Hence, the size of each Pixel was measured as 4.70 μm.

2.5 Viscoelasticity quantification

The hydrogel was assumed to be a Kelvin-Voigt medium that is viscoelastic, isotropic, and homogeneous. Therefore, the SAW propagating in this material exhibited a dispersion behaviour, showing different phase velocities at different frequency components. The air-pulse induced impulse SAW propagated along the surface of the hydrogels horizontally. The upper boundary of the hydrogel was extracted and flattened, then the phase difference of the 20 axial pixels (~94 μm in depth) below the boundary were averaged for SNR enhancement purpose. The axial displacement was calculated from the phase difference between two consecutive A-lines ($\Delta\varphi(x, z, t)$) according to the following equation [49]

$$u_Z(x,z,t) = \frac{\Delta\varphi(x,z,t) * \lambda}{4\pi n} \quad (1)$$

Where λ is the central wavelength of laser source, n is the refractive index of the medium. The axial displacement of ~1.60 mm lateral distance next to the air-pulse excitation point with time constructed the spatial-temporal displacement map. A Gaussian filter for each lateral position was applied to the spatial-temporal displacement map to remove the low frequency background noise. The wavenumber-frequency map was then obtained from the spatial-temporal displacement map by the 2D discrete fast Fourier transform (FFT). The intensity-frequency curve was derived from the wavenumber-frequency map via calculating the maximal intensity of each frequency. The frequency with the highest elastic wave energy corresponded to the central frequency f_c. The phase velocity intensity map was generated by computing the phase velocities of the surface wave at each frequency through Equation 2 [50]

$$C_p = \frac{\omega}{k} \quad (2)$$

Where C_p is the phase velocity. ω represents the angular frequency and k is the wavenumber. The phase velocity dispersion curve was extracted through the maximal intensity of the phase velocity at each frequency. Then, the dispersion curve at a frequency range between 600 Hz and 900 Hz was selected, as it was greater than the highest central frequency of the impulse SAW (more details regarding frequency range selection can be found in Figure S1, Supporting

This article is protected by copyright. All rights reserved.

information). Finally, the dispersion curve was iterated into a Rayleigh wave dispersion model (Equation 3) [35] to estimate the shear modulus and the shear viscosity.

$$C_R(\omega) = \left(\frac{0.87+1.12\upsilon}{1+\upsilon}\right)\sqrt{\frac{2(\mu_1^2+\omega^2\mu_2^2)}{\rho(\mu_1+\sqrt{\mu_1^2+\omega^2\mu_2^2})}} \quad (3)$$

Where C_R is the SAW phase velocity, μ_1 and μ_2 represent the shear modulus and shear viscosity, υ represents Poisson's ratio, ρ is the mass density, and ω denotes the angular frequency. In our study, the hydrogels were immersed and retained moisture in the culture media, which could be deemed to have similar behaviours as rubble-like materials. The Poisson's ratio υ of the hydrogels was assumed as 0.5 [51]. The hydrogel density ρ was assumed as that of the water at 37 °C (993 kg/m^3) [52].

The relationship between elastic modulus (Young's modulus, E) and shear modulus (μ_1) [53] is known as

$$E = 2\mu_1(1+\upsilon) \quad (4)$$

Where E is the elastic modulus of the material. υ is the Poisson's ratio. For the hydrogels, an incompressible elastic model can be considered where the shear modulus (μ_1) is proportional to the elastic modulus (E), according to the expression $E = 3\mu_1$. All the data processing was performed using MATLAB (R2020b, The MathWorks Inc., Massachusetts, USA). The data processing steps for the cell-seeded hydrogels with initial collagen concentration of 5 mg/ml on day 7 are demonstrated in Figure S2 (Supporting information).

2.6 Morphological analysis of fibres

Collagen fibres not only forms fibrillar networks to build and reinforce tissues, but also regulate cell proliferation, migration, and differentiation [54]. The matrix stiffness of the hydrogels can be easily tuned by changing the fibre density [25, 26]. However, the relationship between collagen fibres and viscosity of cell-seeded hydrogel is still unclear. To explore this relationship, scanning electron microscopy (SEM) was employed to obtain high-resolution images of the fibres in dehydrated cell-seeded hydrogels on day 3 and day 11. The hydrogels were prepared

This article is protected by copyright. All rights reserved.

Accepted Article

Accepted Article

for SEM imaging by the following process. The hydrogels were fixed with 4% paraformaldehyde in PBS at room temperature for 1 h. Then, these hydrogels were washed three times with 2.5% glutaraldehyde in 0.1M cacodylate buffer pH 7.2 and immersed into this buffer solution until the next step. The fixed hydrogels were dehydrated with critical point drying (Bal-Tec CPD 030 critical point dryer, Micro Surface Engineering, Inc., California, USA). Next, the dehydrated hydrogels were carefully torn apart with a tweezer to face up the cross-section of the gel. Finally, the dried hydrogels were mounted on the SEM sample stabs with carbon tape and sputter-coated with Au/Pd to a thickness of 10 nm by a coater (Cressington 208HR, Cressington Scientific Instruments Ltd., Watford, UK). The coated specimens were imaged at 5 kilovolt (kV) and magnification of 80,000× by a field emission SEM (JSM-7400F, Japan Electron Optics Laboratory Company, Tokyo, Japan).

To quantify the variations in the morphology of collagen fibres in the cell-seeded hydrogels over time, fibre diameter histograms were constructed by analysing four 1.47 μm × 1.15 μm (length × width) regions from each of two 40,000 × SEM images (original size of 2.95 μm × 2.30 μm) of the cell-seeded hydrogels with three different initial collagen concentrations on day 3 and day 11 (The representative 40,000 × images with segmentation are attached in Figure S3). The morphological properties of the fibres were extracted by the following processes. First, a Hessian filter was applied to binarize the SEM images. Then, the skeletons of all the fibres were obtained in the binary images. The Euclidean distances perpendicular to the skeletons were calculated, regarded as the fibre diameters. In the histograms, the fibre counts were converted to the frequency of occurrences, and the pixels were converted to standard units of length according to the scale bar of the SEM image. The mean value of the fibre diameters was measured from the histograms. The range of the fibre diameters was extracted from the difference between the maximum and minimum values of the diameters in the histograms. The fibre density was obtained from the pixel numbers of the fibres in the binary images over the whole pixel numbers of the images.

This article is protected by copyright. All rights reserved.

Accepted Article

3 RESULTS AND DISCUSSION

3.1 Cell confluency and morphology in hydrogels

The morphology and confluency of keratocytes in the 3 mg/ml, 5 mg/ml, and 7 mg/ml hydrogels on day 3, day 7, day 11, with a magnification of 100× are shown (Figure 2). The results indicate that hydrogels with a lower initial collagen concentration showed a greater increase in cell proliferation when compared to hydrogels with a higher initial collagen concentration. The hydrogels with initial collagen concentration of 3 mg/ml proliferated at the highest rate over 11 days, compared to the 5 mg/ml and the 7mg/ml hydrogels. In the 5 mg/ml hydrogels, an obvious increase in cell number was also observed from day 3 to day 11. By contrast, 7 mg/ml hydrogels exhibited a slow rate of cell proliferation and less change in cell population between 7 and 11 days.

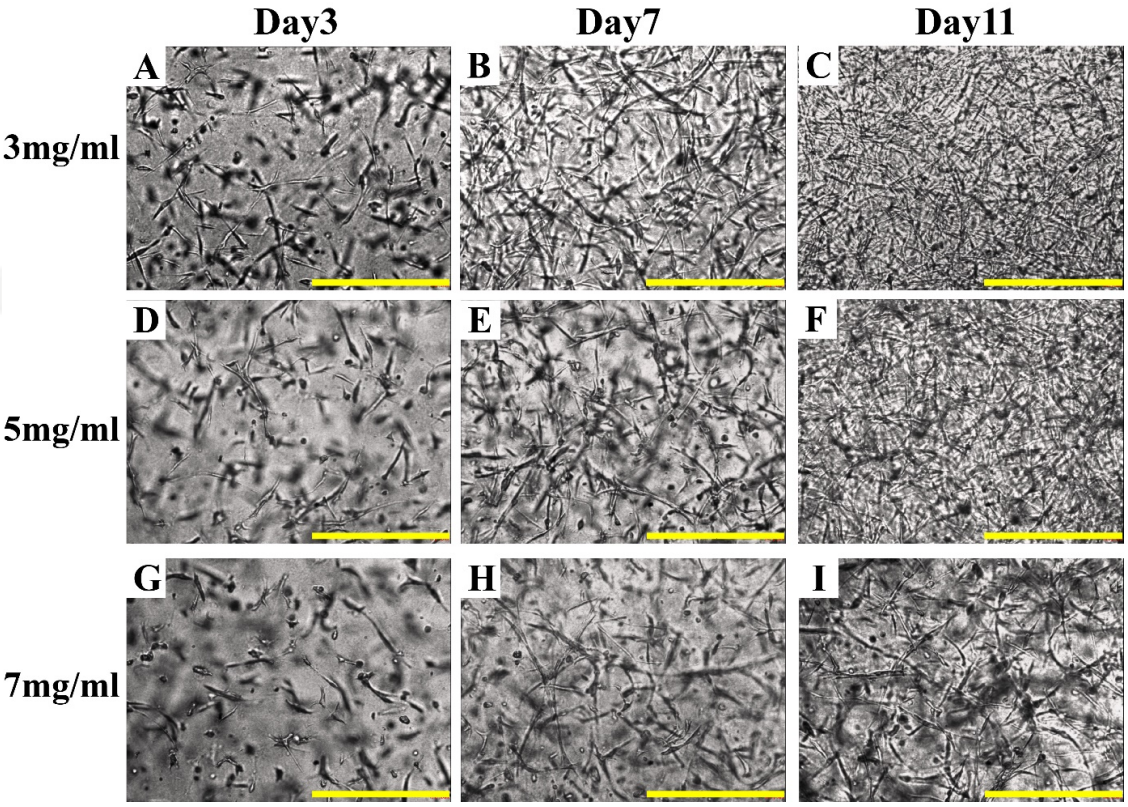

Figure 2. Representative light microscopic images of keratocytes in cell-seeded hydrogels with initial collagen concentrations of 3 mg/ml (A, B, C), 5 mg/ml (D, E, F), and 7 mg/ml (G, H, J) on day 3, day 7 and day 11. The scale bar is 500 μm.

This article is protected by copyright. All rights reserved.

Accepted Article

3.2 Central thickness of hydrogels

Figure 3 demonstrates an example of the central thickness measurement of the cell-seeded hydrogels and no cell controls with initial concentration of 3 mg/ml on day 3, day 7 and day 11. The central thickness of the centre cross-sectional plane of the hydrogels was examined over the culture period (Figure 4). The central thickness of the no cell controls with collagen concentrations of 3 mg/ml, 5 mg/ml, 7 mg/ml was stable at about 1.61 mm, 1.77 mm, and 1.92 mm. The cell-seeded hydrogels with a lower collagen concentration decreased in central thickness quicker than those with a higher collagen concentration (Figure 4A-C). Quantitatively, the central thickness of the cell-seeded hydrogels with initial collagen concentration of 3 mg/ml dropped from 1.45 ± 0.14 mm on day 1 to 0.55 ± 0.08 mm on day 11, with a decrease by 62% (Figure 4A). The 5 mg/ml cell-seeded hydrogels showed an obvious decrease in the central thickness between day 5 at 1.74 ± 0.03 mm and day 11 at 1.30 ± 0.07 mm, with a contraction by 25% (Figure 4B). The hydrogels with initial collagen concentration of 7 mg/ml showed less change in the central thickness during this period, from a starting value of 1.95 ± 0.11 mm to a final value of 1.86 ± 0.07 mm, corresponding to a 5% contraction of the initial central thickness (Figure 4C).

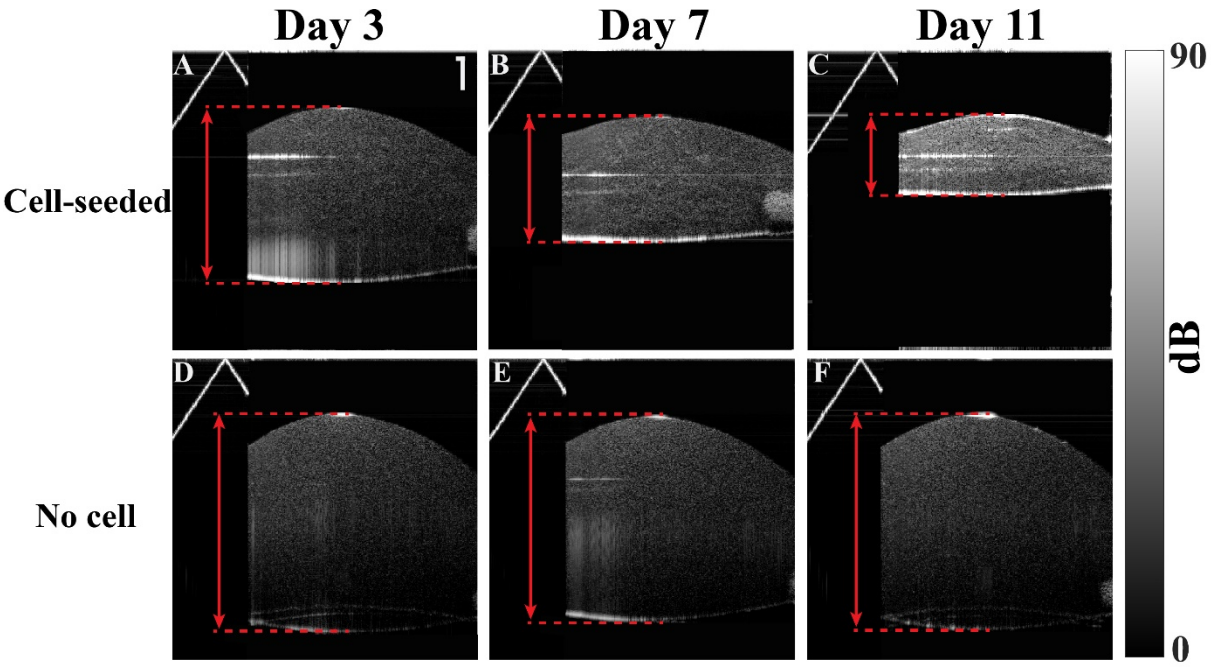

This article is protected by copyright. All rights reserved.

Figure 3. Representative central cross-sectional OCT structure images of hydrogels with initial concentration of 3 mg/ml on day 3 (A, D), day 7 (B, E) and day 11 (C, F). The top and bottom red dotted lines are the peak and the bottom of the hydrogel sample respectively. The red solid double-headed arrows line represents the central thickness of the hydrogel sample. The scale bar is 200 μm.

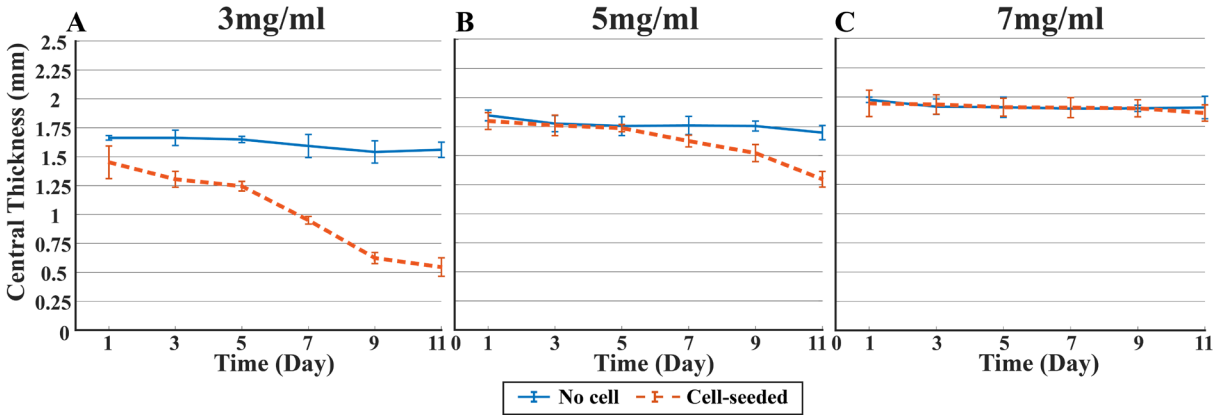

Figure 4. Central thickness of hydrogels with initial collagen concentrations of 3 mg/ml (A), 5mg/ml (B) and 7 mg/ml (C).

3.3 Viscoelastic properties of hydrogels

The final average impulse SAW phase velocity dispersion curves for all the hydrogels at different time-points during an 11-day culture period are displayed in Figure S4 (Supporting information). Based on this, the viscoelastic properties including elastic modulus and viscosity of the hydrogels with initial collagen concentrations (3 mg/ml, 5 mg/ml, 7 mg/ml) were monitored over 11 days in culture, as shown in Figure 5. The results indicated that the hydrogels with lower initial collagen concentrations had a greater rate of increase in the elastic modulus (Figure 5A-C) and viscosity (Figure 5D-F) with time. The elastic modulus of the cell-seeded hydrogels with initial collagen concentration of 3 mg/ml substantially increased from 2.51 ± 0.12 kPa on day 1 to 5.30 ± 0.22 kPa on day 11, while the viscosity had a great increase from 0.07 ± 0.01 Pa·s to 0.32 ± 0.01 Pa·s. The increment was 111% and 357% respectively. For 5 mg/ml cell-seeded hydrogels, the elastic modulus, and the viscosity both experienced a significant increase between day 5 (3.12 ± 0.06 kPa; 0.10 ± 0.01 Pa·s) and day 11 (4.87 ± 0.05

This article is protected by copyright. All rights reserved.

Accepted Article

kPa; 0.31 ± 0.03 Pa·s), with an increase by 56% and 210% respectively. The elastic modulus and the viscosity of 7 mg/ml hydrogels were 5.19 ± 0.23 kPa and 0.24 ± 0.02 Pa·s on day 1. Then, the parameters respectively increased by 0.32 kPa (6%) and 0.06 Pa·s (25%) by day 11. By comparison, the viscoelasticity of the controls with initial concentrations of 3 mg/ml, 5mg/ml and 7 mg/ml were approximately stable in the culture period, with elastic modulus of ~2.10 kPa, ~2.80 kPa and ~4.80 kPa and viscosity of ~0.05 Pa·s, ~0.09 Pa·s and ~0.25 Pa·s.

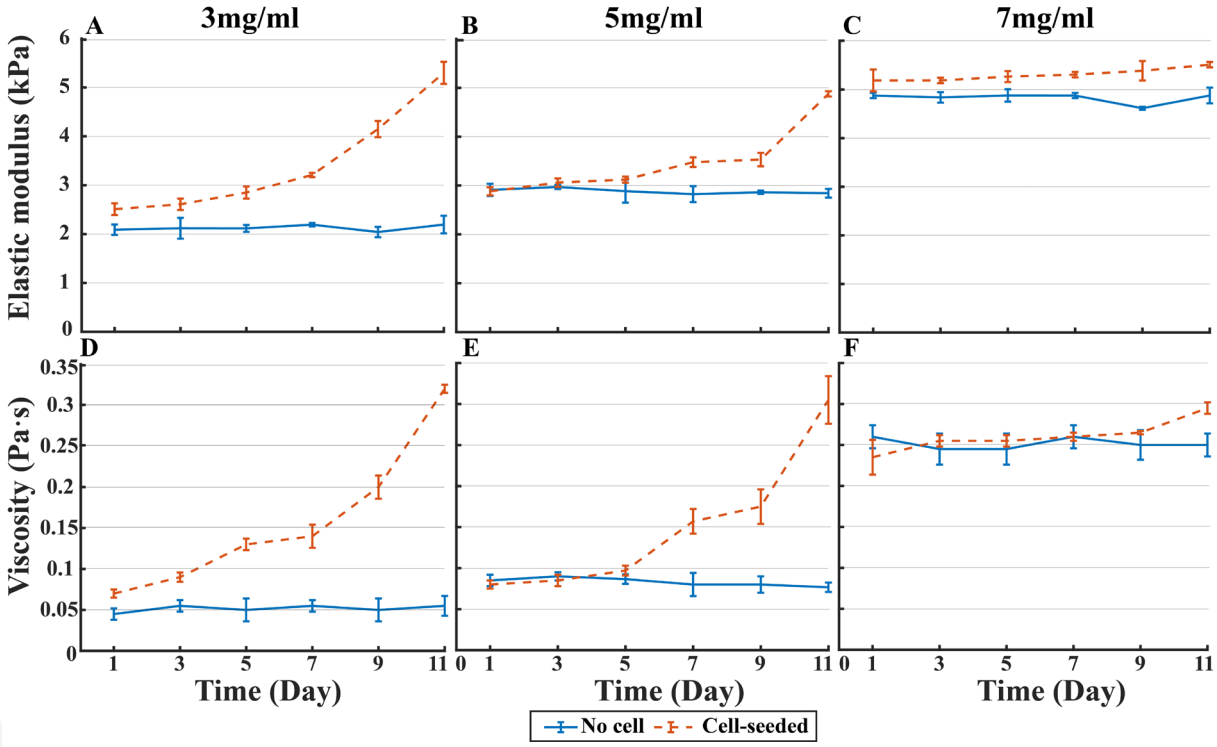

Figure 5. Elastic modulus (A-C) and viscosity (D-F) of hydrogels with initial collagen concentrations of 3mg/ml (A, D), 5 mg/ml (B, E) and 7 mg/ml (C, F).

3.4 Quantification of fibre properties

The cell-seeded hydrogels with initial collagen concentrations of 3 mg/ml, 5 mg/ml and 7 mg/ml were imaged with the SEM system on day 3 and day 11, as demonstrated in Figure 6. On day 3, the apparent fibre bundles were performed in both 3 mg/ml (Figure 6A) and 5 mg/ml hydrogels (Figure 6B). Meanwhile, these hydrogels had larger diameter fibres and larger pore sizes compared to the hydrogels with initial collagen concentration of 7 mg/ml on day 3 (Figure 6C). By contrast, the fibre network in the 7 mg/ml hydrogels was homogeneous, which could

This article is protected by copyright. All rights reserved.

Accepted Article

be seen on day 3 and day 11. Compared with day 3, the collagen fibres in 3 mg/ml (Figure 6D) and 5 mg/ml hydrogels (Figure 6E) demonstrated unbinding of the bonds between the fibres on day 11. The fibre diameters and the pore sizes were substantially decreased as well.

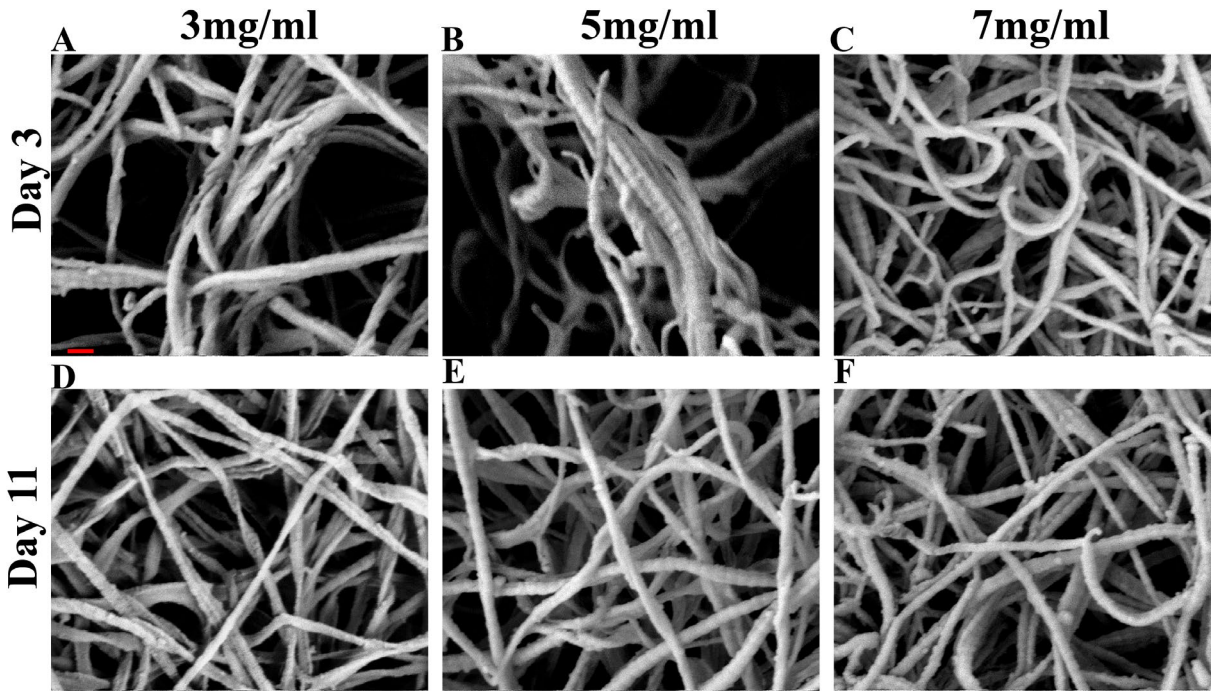

Figure 6. SEM images shown fibres in hydrogels with initial collagen concentrations of 3 mg/ml (A, D), 5 mg/ml (B, E), 7 mg/ml (C, F) on day 3 and day 11. The magnification is 80,000×. The scale bar represents 100 nm.

Figure 7 presents the fibre diameter histograms constructed from the SEM images. On day 3, the hydrogels with initial concentrations of 3 mg/ml and 5 mg/ml had similar mean values of the fibre diameters of 61.4 ± 10.9 nm and 56.3 ± 4.1 nm respectively, whereas the mean value of the fibre diameters was around 26.4 ± 4.7 nm in the 7 mg/ml hydrogels. Meanwhile, the range of the fibre diameters in the 3 mg/ml and the 5 mg/ml hydrogels was 123.8 ± 11.6, about 4 times larger than that of the 7 mg/ml hydrogels. The fibre density in the 7 mg/ml hydrogels (0.61 ± 0.02) was much higher than that of the hydrogels with two lower initial collagen concentrations (3 mg/ml: 0.52 ± 0.02; 5 mg/ml: 0.51 ± 0.07). On day 11, the hydrogels with three different collagen concentrations demonstrated similar mean values of fibre diameters (3

This article is protected by copyright. All rights reserved.

Accepted Article

mg/ml: 29.4 ± 8.0 nm; 5 mg/ml: 25.6 ± 8.5 nm; 7 mg/ml: 25.5 ± 9.3 nm), range of fibre diameters (3 mg/ml: 36.7 ± 6.7 nm; 5 mg/ml: 32.7 ± 1.4 nm; 7 mg/ml: 30.3 ± 4.0 nm) and fibre density (3 mg/ml: 0.61 ± 0.01; 5 mg/ml: 0.60 ± 0.02; 7 mg/ml: 0.62 ± 0.01%)

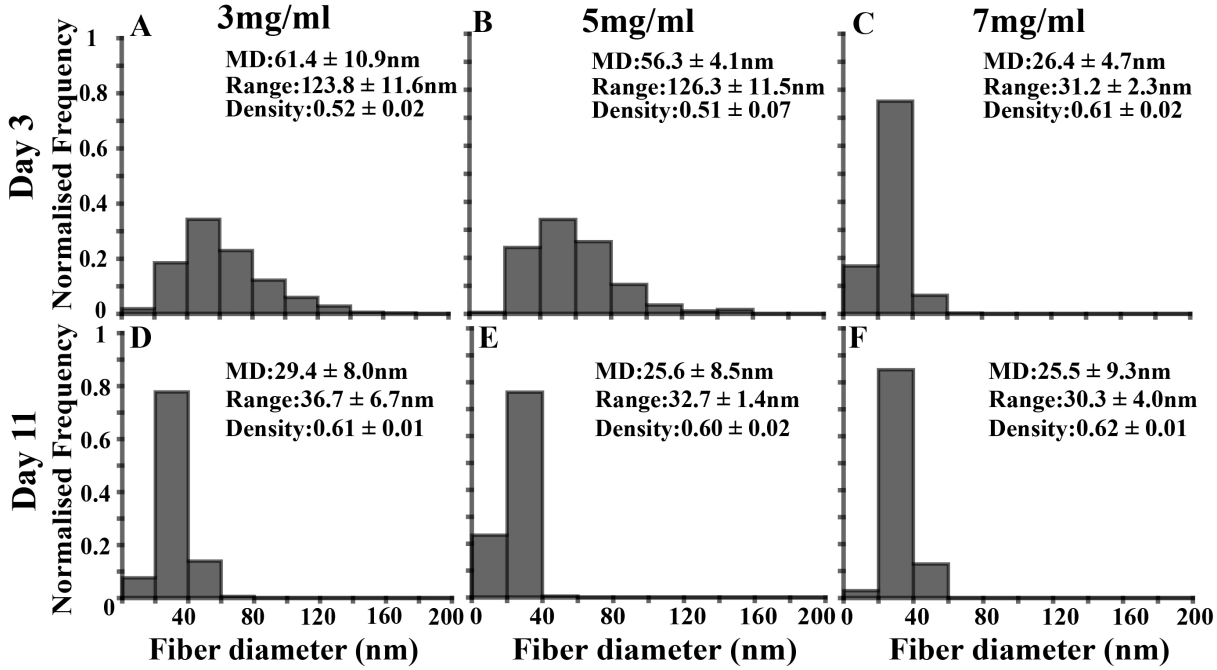

Figure 7. Fibre diameter histograms of hydrogels with initial collagen concentrations of 3 mg/ml (A, D), 5 mg/ml (B, E), and 7 mg/ml (C, F) on day 3 (A-C) and day 11 (D-F) constructed from SEM images. The corresponding collagen fibre diameter and density in SEM images are listed above in each histogram. Eight regions were divided from two SEM images of each cell-seeded hydrogel on day 3 and day 11. MD: Mean diameter.

In this paper, the influence of the interactions between stromal cell and ECM on the viscoelastic properties of reconstructed human corneal stromal models has been demonstrated. The phase stabilised air-pulse induced SAW-OCE system was employed to repeatedly measure the dimension changes and the impulse SAW phase velocity of the hydrogels with different initial collagen concentrations at several time-points over a consecutive 11-day culture period. The impulse SAW phase velocity was fitted into a Rayleigh wave dispersion equation to determine the elastic modulus and the viscosity of the hydrogels. Moreover, to explain the changes in the

This article is protected by copyright. All rights reserved.

Accepted Article

viscoelasticity of the collagen-based hydrogels, the morphology of collagen fibres was discerned and quantified with the SEM system images.

The primary advantages of this study are that (1) a totally non-contact air-pulse system is applied to avoid the contamination of the hydrogels (2) a very small displacement is induced to avert deformation on the hydrogels during the culture period (3) continuous monitoring of the changes takes place in the viscoelastic properties of the hydrogels with different initial collagen concentrations (4) the morphology of the fibres in the hydrogels is perceived and the fibre properties are computed at two different time points.

Compared to other OCE methods, such as ultrasound induced wave-based OCE [55, 56] or piezoelectric transducer (PZT) induced wave-based OCE [57, 58], air-pulse induced wave-based OCE is a totally non-contact detection approach, which is suitable to realise continuous biomechanical measurements of samples.

The central thickness analysis (Figure 4) showed that the hydrogels with a higher collagen concentration experienced a lower rate of decrease in the central thickness compared to the hydrogels with lower concentrations over 11 days. This indicated that the hydrogels with lower collagen concentrations were more contractile due to a weak mechanical resistance during keratocytes contracting the ECM. The changes in the viscoelastic properties of the hydrogels (Figure 5) were mainly due to cell-matrix interactions. Specifically, keratocytes integrate themselves within the hydrogels, attach to the collagen matrix [19], and release ECM products [18] to manipulate the mechanical properties of their surrounding ECM. In turn, the variations in the mechanical properties of the ECM can influence cell behaviours [21-23]. Our data exhibited that increasing the rate of cell proliferation finally led to an increase in elastic modulus and viscosity of the hydrogels over the culture period. The phenomenon could be explained that increasing the number of cells induced a higher cell density in the hydrogels [25, 26]. Afterwards, the increased cell density caused an increase in the amount of force required to contract the collagen matrix throughout the hydrogels. In this process, water content was pushed out of the

This article is protected by copyright. All rights reserved.

Accepted Article

hydrogels [46], leading to a higher overall collagen density and an increase in elastic modulus of the hydrogels. At the same time, greater strains were applied to the fibres in the hydrogels, resulting in higher forces taken by the fibres and fibre bonds as well. Therefore, unbinding of the fibre bonds occurred in turn, inducing an increase in viscosity of the hydrogels [27].

Ahearne *et al.* [44] examined the changes in the elastic modulus of corneal stromal models with initial collagen concentrations of 2.5 mg/ml, 3.5 mg/ml, and 4.5 mg/ml during a 25-day culture period with a spherical indentation method. Their results demonstrated that the elastic modulus of the 2.5 mg/ml hydrogels started with ~2 kPa, then raised to ~5 kPa at the end. In our study, the elastic modulus of the 3 mg/ml hydrogels had a similar value and increasing trend during the culture period. Likewise, the hydrogels with a higher initial collagen concentration had fewer changes in the elastic modulus and thickness. However, our results showed that the hydrogels with initial collagen concentration of 5 mg/ml had a higher elastic modulus value than those of the 4.5 mg/ml hydrogels in their paper. This might be caused by the original concentration of collagen type I. The collagen concentration of our hydrogels was diluted from type I collagen with a concentration of 9.1 mg/ml which was likely of a higher concentration than those they used. Accordingly, more water content was required to compound these hydrogels compared with their study. This could be seen from the dimensional changes of the hydrogels. In their study, the thickness of the 4.5 mg/ml hydrogels with 1×10^5 cells seeded varied from 1.0 mm on day 1 to 0.8 mm on day 25. By contrast, our 5 mg/ml hydrogels experienced a 0.50 mm (28%) decrease in the culture period, which indicated that these hydrogels were more contactable than their hydrogels. We also noticed that the central thickness of the hydrogels with three different collagen concentrations was not consistent on day 1 and 3 mg/ml hydrogels had the lowest central thickness. The reason behind this was that 1 hour was needed for gelation of the hydrogels on a hydrophobic plate in the incubator. As the hydrogels with a lower initial collagen concentration had a weak resistance to contraction, water content reduced faster in these hydrogels inducing lower thickness on day 1. Compared to their study,

This article is protected by copyright. All rights reserved.

Accepted Article

we studied a larger range of collagen concentrations in the hydrogel samples, so we were able to provide more general conclusions. In our study, we also looked at the viscosity of the hydrogels.

Zvietcovich *et al.* [59] reported that a wave-based OCE method to capture an ultrasound induced shear wave inside the hydrogels with different collagen concentrations (2 mg/ml, 5 mg/ml, 6.7 mg/ml and 10.6 mg/ml). The collagen concentration of the hydrogels was regulated by changing the mass of the collagen by dehydration. Their results showed that the relative viscosity values of the hydrogels with increasing collagen concentrations were comparable with ours, in addition to an increasing trend of hydrogel viscosity with increasing collagen concentrations. In their study, the 2 mg/ml and the 5 mg/ml hydrogels also had a semblable initial viscosity of ~0.1 NP/mm/kHz, much less than that of 7 mg/ml hydrogels (~0.18 NP/mm/kHz). However, their excitation method damaged the samples so that a continuous mechanical property monitoring could not be realised. In addition, the elastic modulus was not reported to have any correlations with different initial collagen concentrations of the hydrogels based on their dispersion model. In fact, many studies [31-33] reported that hydrogels with higher collagen concentrations had higher initial values of elastic modulus and viscosity than hydrogels with lower initial collagen concentrations by using rheological tests.

Another innovative point of this study was that changes in the morphological properties of the hydrogels' fibres were analysed by SEM imaging. SEM system has been used in a number of studies to observe collagen fibres in the hydrogels [60-62] as it has high resolution in microstructure measurement. In our study, the properties of the collagen fibres in the hydrogels analysed from their SEM images confirmed the viscoelasticity of the hydrogels detected with SAW-OCE system. Previous studies [25, 26] reported that hydrogels with a higher fibre density had higher matrix stiffness than hydrogels with a lower fibre density. In respect to the viscosity, a faster rate of contraction of the surrounding matrix led to an added strain exerted on the cells and fibres in hydrogels. In conjunction with the proposition from Nam *et al.* [27], a greater force

This article is protected by copyright. All rights reserved.

Accepted Article

increases the probability of unbinding, and this unbinding of fibres can lead to strain-enhanced stress relaxation. Higher forces on the fibres and fibre bonds resulted in faster unbinding because of the enhanced strains. In our study, the cell-matrix interactions resulted in contraction of the hydrogels generated increased forces applied on the fibre bonds, leading to an unbinding of the fibre bonds over time, especially in hydrogels with lower initial collagen concentrations. The decrease in the mean value of and the range of the fibre diameters reflected the unbinding of the fibre bonds over the culture period.

The morphological changes of collagen fibres in hydrogels with different viscoelastic properties resulting from the cell-matrix interactions have never been studied. We validated our results by comparing them to the study of Raub *et al.*[61]. They observed collagen fibres in hydrogels formed at four different polymerization temperatures by SEM and measured the viscoelastic properties of the hydrogels with a rheometer. Both the shear modulus and shear viscosity of the hydrogels raised with the increasing polymerization temperatures. Importantly, their SEM images also demonstrated that the unbinding of the hydrogels' fibre bonds occurred during an increase in elastic modulus and viscosity of the hydrogels. In our study, the unbinding of bonds between fibres was observed in the 3 mg/ml and 5 mg/ml hydrogels from day 3 to day 11. In comparison to the quantification method, measuring Euclidean distance transform along the skeletons of the collagen fibres was more objective than the hand-measurement in their study.

Currently, a critical limitation of tissue-engineered materials is that no studies have been performed on the fibre structure examination of hydrogels with collagen concentration >4 mg/ml since collagen hydrogels below this concentration are widely used. However, the hydrogels with collagen concentration less than 4 mg/ml have not been capably replicated to the properties of *in vivo* tissues, largely because of insufficient structural integrity to support microfabrication [63]. Thus, the use of the higher concentration hydrogels for mimicking *in vivo* tissues will become a new trend and full viscoelastic characterisation of these hydrogels is essential.

This article is protected by copyright. All rights reserved.

Accepted Article

Accepted Article

In our study, with decreasing thickness of hydrogels, especially the 3 mg/ml cell-seeded hydrogels from day 7 to day 11, the dominating elastic wave might change to Lamb wave. It was because the thickness of the hydrogels was close to the order of the elastic wavelength [64]. The dominating antisymmetric propagation mode was generated, as the direction of air-steam stimulated from air-pulse system was close to the hydrogel surface normal [39]. However, the phase velocity of Lamb wave converges to the surface wave velocity (Rayleigh) in the high frequency of asymmetric mode A_0 for the case of sample with air-medium (free) boundaries [35]. Previous studies [57, 65] characterised corneal viscoelasticity based on this elastic wave theory to calculate Lamb wave velocity in a high-frequency (greater than central frequency) through a Rayleigh wave equation. Thus, even though the dominating wave changed to Lamb wave due to the reduced thickness of the hydrogels, the viscoelastic parameters were still able to be estimated by fitting the phase velocity in the high frequency range into the Rayleigh wave dispersion equation.

The limitation of this work was that although the acquisition time was controlled as short as possible, it was restricted by the air-pulse repetition rate [66]. The low repetition rate of the air-pulse system limited the OCT scanning speed. In future, a higher repetition rate of our air-pulse system will be developed by further improving the control circuit. Moreover, as the culture medium had to be removed during the acquisition and 4-time repeats at each hydrogel sample, water content inside the hydrogels with lower initial collagen concentrations was probably slightly evaporated by the air stream. As a result, the hydrogels' contraction may be enhanced, which led to an increase in elastic modulus and viscosity. However, the dimensional changes (Figure 4) and viscoelasticity changes (Figure 5) of the no cell controls indicated that the evaporation of the water content within the hydrogels caused by the air stream could be ignored. In future, the current stromal hydrogel model will be developed to have the epithelial and endothelial layers, which can better mimic real human corneal structure. In addition, a traumatic injury will be introduced to the new corneal model. The cell behaviours and the morphological changes of the fibres will be investigated during wound healing *in vitro* at different time-points. As it includes multiple layers, a layered new wave propagation model will be applied for biomechanical property analysis [39, 67].

4 CONCLUSIONS

In conclusion, the influence of the interactions between stromal cell and stromal ECM on the viscoelastic property of corneal stroma models can be seen in this study. The changes in the

This article is protected by copyright. All rights reserved.

dimensions and the viscoelastic properties of the hydrogels with different initial collagen concentrations were monitored by a non-destructive air-pulse induced SAW-OCE method over a consecutive 11-day culture period. In addition, the corresponding morphological changes in the hydrogels' fibres were quantified with SEM images. The findings enhance our understanding on change in corneal viscoelasticity. Moreover, the outcomes can act as a guide to fabricate collagen matrix with tuneable properties in mechanobiological investigations.

ACKNOWLEDGMENTS

The authors would like to thank Dr. Alan Prescott for the preparation of the SEM samples and Dr. Yongchang Fan for operating the SEM system. This work was supported by National Centre for the Replacement Refinement and Reduction of Animals in Research (10945a_CRT).

CONFLICT OF INTEREST

The authors declare no financial or commercial conflict of interest.

REFERENCES

[1] D. W. DelMonte, T. Kim *Journal of Cataract & Refractive Surgery*. **2011**, *37*, 588-598.
[2] S. Kling, F. Hafezi *Ophthalmic and Physiological Optics*. **2017**, *37*, 240-252.
[3] I. S. Nash, P. R. Greene, C. S. Foster *Experimental eye research*. **1982**, *35*, 413-424.
[4] J. H. Krachmer, R. S. Feder, M. W. Belin *Survey of ophthalmology*. **1984**, *28*, 293-322.
[5] S. Shah, M. Laiquzzaman, R. Bhojwani, S. Mantry, I. Cunliffe *Investigative ophthalmology & visual science*. **2007**, *48*, 3026-3031.
[6] R. Kopito, T. Gaujoux, R. Montard, O. Touzeau, C. Allouch, V. Borderie, L. Laroche *Acta ophthalmologica*. **2011**, *89*, e225-e230.
[7] D. H. Glass, C. J. Roberts, A. S. Litsky, P. A. Weber *Invest Ophthalmol Vis Sci*. **2008**, *49*, 3919-3926.
[8] Y. Goldich, Y. Barkana, Y. Morad, M. Hartstein, I. Avni, D. Zadok *Cornea*. **2009**, *28*, 498-502.
[9] M. Gkika, G. Labiris, A. Giarmoukakis, A. Koutsogianni, V. Kozobolis *Graefe's Archive for Clinical and Experimental Ophthalmology*. **2012**, *250*, 565-573.
[10] S. Wang, C. E. Ghezzi, R. Gomes, R. E. Pollard, J. L. Funderburgh, D. L. Kaplan *Biomaterials*. **2017**, *112*, 1-9.
[11] K. S. Anseth, C. N. Bowman, L. BrannonPeppas *Biomaterials*. **1996**, *17*, 1647-1657.
[12] K. M. Meek *Biophysical Reviews*. **2009**, *1*, 83-93.
[13] T. Ihanamäki, L. J. Pelliniemi, E. Vuorio *Progress in retinal and eye research*. **2004**, *23*, 403-434.
[14] P. Fournié, G. M. Gordon, D. R. Ledee, C. J. Roberts, M. E. Fini *BRIGHTBILL, FS, PJ MCDONNELL. Corneal surgery: theory, technique, and tissue*. **2008**, 33-44.

This article is protected by copyright. All rights reserved.

Accepted Article

Accepted Article

[15] A. Kim, N. Lakshman, D. Karamichos, W. M. Petroll *Investigative ophthalmology & visual science*. **2010**, *51*, 864-875.
[16] M. E. Smithmyer, L. A. Sawicki, A. M. Kloxin *Biomaterials science*. **2014**, *2*, 634-650.
[17] K. M. Park, D. Lewis, S. Gerecht *Annual review of biomedical engineering*. **2017**, *19*, 109-133.
[18] Z. A. Saddiq, J. C. Barbenel, M. H. Grant *Journal of Biomedical Materials Research Part A: An Official Journal of The Society for Biomaterials, The Japanese Society for Biomaterials, and The Australian Society for Biomaterials and the Korean Society for Biomaterials*. **2009**, *89*, 697-706.
[19] K. Takakuda, H. Miyairi *Biomaterials*. **1996**, *17*, 1393-1397.
[20] E. Bell, B. Ivarsson, C. Merrill *Proceedings of the National Academy of Sciences*. **1979**, *76*, 1274-1278.
[21] V. L. Cross, Y. Zheng, N. W. Choi, S. S. Verbridge, B. A. Sutermaster, L. J. Bonassar, C. Fischbach, A. D. Stroock *Biomaterials*. **2010**, *31*, 8596-8607.
[22] M. Levy-Mishali, J. Zoldan, S. Levenberg *Tissue Engineering Part A*. **2009**, *15*, 935-944.
[23] N. Yamamura, R. Sudo, M. Ikeda, K. Tanishita *Tissue engineering*. **2007**, *13*, 1443-1453.
[24] O. Chaudhuri, L. Gu, D. Klumpers, M. Darnell, S. A. Bencherif, J. C. Weaver, N. Huebsch, H. P. Lee, E. Lippens, G. N. Duda, D. J. Mooney *Nat Mater*. **2016**, *15*, 326-334.
[25] A. J. Licup, S. Münster, A. Sharma, M. Sheinman, L. M. Jawerth, B. Fabry, D. A. Weitz, F. C. MacKintosh *Proceedings of the National Academy of Sciences*. **2015**, *112*, 9573-9578.
[26] S. Kreger, B. Bell, J. Bailey, E. Stites, J. Kuske, B. Waisner, S. Voytik‐Harbin *Biopolymers: Original Research on Biomolecules*. **2010**, *93*, 690-707.
[27] S. Nam, K. H. Hu, M. J. Butte, O. Chaudhuri *Proc Natl Acad Sci U S A*. **2016**, *113*, 5492-5497.
[28] J. M. Patel, B. C. Wise, E. D. Bonnevie, R. L. Mauck *Tissue Engineering Part C: Methods*. **2019**, *25*, 593-608.
[29] B. Xu, H. Li, Y. Zhang *Biomatter*. **2013**, *3*.
[30] R. Kocen, M. Gasik, A. Gantar, S. Novak *Biomed Mater*. **2017**, *12*, 025004.
[31] C. Valero, H. Amaveda, M. Mora, J. M. Garcia-Aznar *PLoS One*. **2018**, *13*, e0195820.
[32] M. Shayegan, N. R. Forde *PLoS One*. **2013**, *8*, e70590.
[33] P. Sánchez-Cid, M. Jiménez-Rosado, V. Perez-Puyana, A. Guerrero, A. Romero *Polymers*. **2021**, *13*, 632.
[34] Z. Yaqoob, J. Wu, C. Yang *Biotechniques*. **2005**, *39*, S6-S13.
[35] M. A. Kirby, I. Pelivanov, S. Song, L. Ambrozinski, S. J. Yoon, L. Gao, D. Li, T. T. Shen, R. K. Wang, M. O'Donnell *Journal of biomedical optics*. **2017**, *22*, 121720.
[36] V. Y. Zaitsev, A. L. Matveyev, L. A. Matveev, A. A. Sovetsky, M. S. Hepburn, A. Mowla, B. F. Kennedy *Journal of biophotonics*. **2021**, *14*, e202000257.
[37] S. Wang, K. V. Larin, J. Li, S. Vantipalli, R. Manapuram, S. Aglyamov, S. Emelianov, M. Twa *Laser Physics Letters*. **2013**, *10*, 075605.
[38] Z. Han, M. Singh, S. R. Aglyamov, C.-H. Liu, A. Nair, R. Raghunathan, C. Wu, J. Li, K. V. Larin *Journal of biomedical optics*. **2016**, *21*, 090504.
[39] S. Wang, K. V. Larin *Biomedical optics express*. **2014**, *5*, 3807-3821.
[40] M. Singh, Z. Han, J. Li, S. Vantipalli, S. R. Aglyamov, M. D. Twa, K. V. Larin *Journal of Cataract & Refractive Surgery*. **2018**, *44*, 1023-1031.
[41] Z. Han, J. Li, M. Singh, C. Wu, C.-h. Liu, R. Raghunathan, S. R. Aglyamov, S. Vantipalli, M. D. Twa, K. V. Larin *Journal of the mechanical behavior of biomedical materials*. **2017**, *66*, 87-94.
[42] Z. Han, S. R. Aglyamov, J. Li, M. Singh, S. Wang, S. Vantipalli, C. Wu, C.-h. Liu, M. D. Twa, K. V. Larin *Journal of biomedical optics*. **2015**, *20*, 020501.
[43] M. Ahearne, Y. Yang, K. Y. Then, K.-K. Liu *British journal of ophthalmology*. **2008**, *92*, 268-271.

This article is protected by copyright. All rights reserved.

Accepted Article

[44] M. Ahearne, S. L. Wilson, K. K. Liu, S. Rauz, A. J. El Haj, Y. Yang *Exp Eye Res*. **2010**, *91*, 584-591.
[45] H. A. Awad, D. L. Butler, M. T. Harris, R. E. Ibrahim, Y. Wu, R. G. Young, S. Kadiyala, G. P. Boivin *Journal of Biomedical Materials Research: An Official Journal of The Society for Biomaterials, The Japanese Society for Biomaterials, and The Australian Society for Biomaterials and the Korean Society for Biomaterials*. **2000**, *51*, 233-240.
[46] M. Ahearne, K.-K. Liu, A. J. El Haj, K. Y. Then, S. Rauz, Y. Yang *Tissue Engineering Part C: Methods*. **2010**, *16*, 319-327.
[47] Y. L. Zhang, Y. T. Ling, D. Zhang, M. K. Wang, C. Purslow, Y. Yang, C. H. Li, Z. H. Huang *Biomedical Optics Express*. **2021**, *12*, 588-603.
[48] P. Schiebener, J. Straub, J. Levelt Sengers, J. Gallagher *Journal of physical and chemical reference data*. **1990**, *19*, 677-717.
[49] R. K. Wang, S. Kirkpatrick, M. Hinds *Applied Physics Letters*. **2007**, *90*, 164105.
[50] K. Zhou, N. Le, Z. Huang, C. Li *Journal of biophotonics*. **2018**, *11*, e201700051.
[51] M. Ahearne, Y. Yang, A. J. El Haj, K. Y. Then, K.-K. Liu *Journal of the Royal Society Interface*. **2005**, *2*, 455-463.
[52] S. Piskounova, R. Rojas, K. Bergman, J. Hilborn *Macromolecular Materials and Engineering*. **2011**, *296*, 944-951.
[53] F. G. Bell in *ENGINEERING GEOLOGY | Rock Properties and Their Assessment, Vol.* (Eds.: R. C. Selley, L. R. M. Cocks, I. R. Plimer), Elsevier, Oxford, **2005**, pp.566-580.
[54] F. Kai, H. Laklai, V. M. Weaver *Trends in cell biology*. **2016**, *26*, 486-497.
[55] K. Zhou, C. Li, S. Chen, G. Nabi, Z. Huang *J Biophotonics*. **2019**, *12*, e201800177.
[56] F. Zvietcovich, J. P. Rolland, K. J. Parker *Journal of Innovative Optical Health Sciences*. **2017**, *10*.
[57] Z. Jin, Y. Zhou, M. Shen, Y. Wang, F. Lu, D. Zhu *Journal of biophotonics*. **2020**, *13*, e201960074.
[58] A. Ramier, B. Tavakol, S. H. Yun *Opt Express*. **2019**, *27*, 16635-16649.
[59] D. D. Sampson, K. V. Larin, S. Wayson, E. Grygotis, J. P. Rolland, K. J. Parker, D. Dalecki, M. Helguera, F. Zvietcovich in Viscoelastic characterization of dispersive media by inversion of a general wave propagation model in optical coherence elastography, Vol. (Ed.^Eds.: Editor), City, **2018**.
[60] A. Pogorelov, I. Selezneva *Bulletin of experimental biology and medicine*. **2010**, *150*, 153-156.
[61] C. B. Raub, V. Suresh, T. Krasieva, J. Lyubovitsky, J. D. Mih, A. J. Putnam, B. J. Tromberg, S. C. George *Biophys J*. **2007**, *92*, 2212-2222.
[62] K. A. Jansen, A. J. Licup, A. Sharma, R. Rens, F. C. MacKintosh, G. H. Koenderink *Biophysical journal*. **2018**, *114*, 2665-2678.
[63] E. E. Antoine, P. P. Vlachos, M. N. Rylander *Tissue Engineering Part B: Reviews*. **2014**, *20*, 683-696.
[64] T.-M. Nguyen, M. Couade, J. Bercoff, M. Tanter *IEEE transactions on ultrasonics, ferroelectrics, and frequency control*. **2011**, *58*, 2305-2315.
[65] Z. Jin, R. Khazaeinezhad, J. Zhu, J. Yu, Y. Qu, Y. He, Y. Li, T. E. G. Alvarez-Arenas, F. Lu, Z. Chen *Biomedical optics express*. **2019**, *10*, 6272-6285.
[66] S. Wang, K. V. Larin *Journal of biophotonics*. **2015**, *8*, 279-302.
[67] F. Zvietcovich, P. Pongchalee, P. Meemon, J. P. Rolland, K. J. Parker *Nature communications*. **2019**, *10*, 1-13.

SUPPORTING INFORMATION

Additional supporting information can be found in the online version of the article at the publisher's website.

This article is protected by copyright. All rights reserved.